Petroleum Science 19 (2022) 1641–1652

Contents lists available at ScienceDirect

Petroleum Science

journal homepage: www.keaipublishing.com/en/journals/petroleum-science

Review Paper

Determination of dynamic capillary effect on two-phase flow in porous media: A perspective from various methods

Jian-Chao Cai [a, b], Yin Chen [b], Jun-Cheng Qiao [a], Liu Yang [c], Jian-Hui Zeng [a], Chen-Hao Sun [a, *]

[a] State Key Laboratory of Petroleum Resources and Prospecting, China University of Petroleum, Beijing, 102249, PR China
[b] Institute of Geophysics and Geomatics, China University of Geosciences, Wuhan, 430074, Hubei, PR China
[c] State Key Laboratory for Geomechanics and Deep Underground Engineering, China University of Mining and Technology (Beijing), Beijing, 100083, PR China

ARTICLE INFO

Article history:
Received 20 October 2021
Received in revised form
20 January 2022
Accepted 21 January 2022
Available online 27 January 2022

Edited by Yan-Hua Sun

Keywords:
Dynamic capillary effect
Capillary pressure
Two-phase flow
Modeling method

ABSTRACT

The relationship between capillary pressure and saturation plays a critical role in the characterization of two-phase flow and transport in aquifers and oil reservoirs. This relationship is usually determined under the static condition, where capillary pressure is the only function of saturation. However, considerable experiments have suggested that the dependence of capillary pressure on desaturation rate is under the dynamic condition. Thus, a more general description of capillary pressure that includes dynamic capillary effect has been approved widely. A comprehensive understanding of the dynamic capillary effect is needed for the investigation of the two-phase flow in porous media by various methods. In general, dynamic capillary effect in porous media can be studied through the laboratory experiment, pore- to macro-scale modeling, and artificial neural network. Here, main principle and research procedures of each method are reviewed in detail. Then, research progress, disadvantages and advantages are discussed, respectively. In addition, upscaling study from pore- to macro-scale are introduced, which explains the difference between laboratory experiment and pore-scale modeling. At last, several future perspectives and recommendations for optimal solution of dynamic capillary effect are presented.

1. Introduction

The constitutive relationship between capillary pressure (P_c) and wetting phase saturation (S_w) is the foundation for the characterization of immiscible two-phase flow in porous media (Cai and Yu, 2011; Cai et al., 2014, 2021; Ansarinasab and Jamialahmadi, 2016; Gao et al., 2018; Liu et al., 2019). P_c is regarded as the pressure difference between the average non-wetting (P^a_{nw}) and wetting (P^a_w) phases (Bear and Verruijt, 1987). In general, the average P_c–S_w relationship is determined under the static condition where desaturation (Zhou et al., 2021) rate ($\partial S/\partial t$) is assumed as zero. A diagrammatic sketch of the non-linear and static P_c–S_w relation is given in Fig. 1a. Mathematically, the relation is described as:

$$P^a_{nw} - P^a_w = P_c(S_w) = f(S_w) \quad (1)$$

However, static representation by Eq. (1) leads to a poor prediction of two-phase flow behavior, especially for the case of high flow velocities (the injected phase) as shown in experimental data (Topp et al., 1967; Wildenschild et al., 2001; Oung et al., 2005; Camps-Roach et al., 2010; Sakaki et al., 2010). In this case, P_c is dependent not only on the saturation but also on the desaturation rate $\partial S/\partial t$. The saturation–rate dependency during two-phase flow at non-equilibrium condition is called the "dynamic capillary effect". Several phenomena have been reported as responsible factors for the presence of a dynamic capillary effect, such as air and/or water entrapment, pore water blockage, air entry effect, and dynamic contact angle (Friedman, 1999; Wildenschild et al., 2001). The difference between dynamic and static P_c–S_w curves was firstly revealed by Topp et al. (1967). In their experiment, the dynamic capillary pressure is always larger than the static one (Fig. 1b). Dynamic capillary coefficient τ, which refers as the relaxation time

* Corresponding author.
E-mail address: chenhao.sun@cup.edu.cn (C.-H. Sun).

https://doi.org/10.1016/j.petsci.2022.01.017

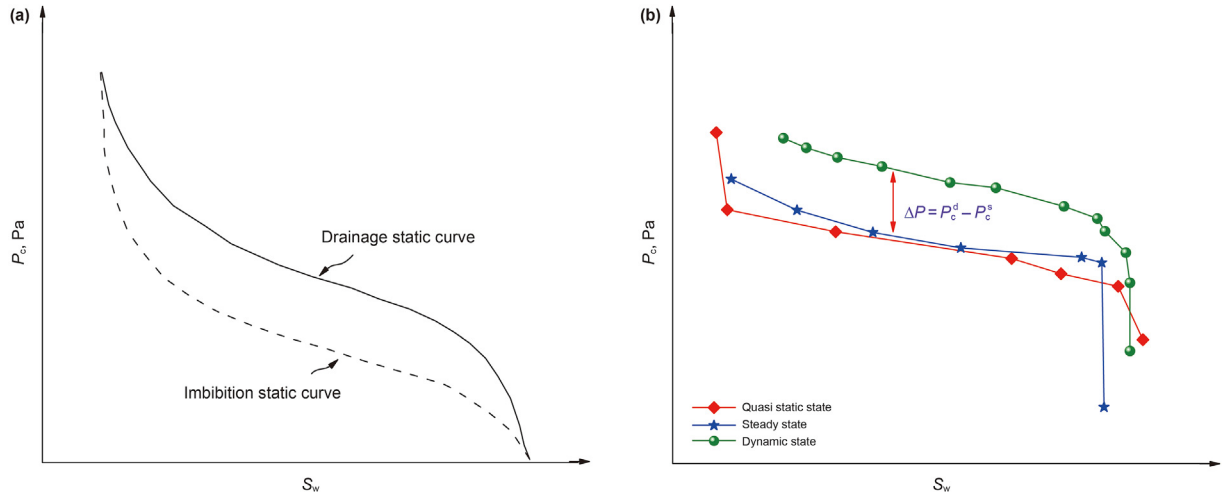

Fig. 1. The schematic of P_c–S_w curves: (**a**) static curves (P_c is only related to S_w); (**b**) dynamic curves (P_c is related to S_w and its change rate over time) (Topp et al., 1967).

or damping coefficient, is a parameter for directly measuring the dynamic capillary effect. Specifically, τ controls the speed of reaching the equilibrium state. A larger value of τ indicates that more time is required for flow to reach the equilibrium after a disturbance (Li et al., 2018). More detailed summarizations on influential factors of the dynamic capillary effect, the influencing mechanism and tendency of each factor could consult the recent review work by Chen et al. (2022).

From the perspective of research methods, this work mainly reviews laboratory experiments, pore- to macro-scale modeling, and artificial neural network (ANN). The research procedures of each method for determining the dynamic capillary effect are introduced. For pore-scale modeling, the application condition, disadvantages and advantages of lattice Boltzmann method (LBM), pore network model (PNM) and pore-unit assembly model are discussed systematically. For macro-scale modeling, the innovations (taking different factors into account) of each model are presented, which contributes to adopting appropriate model in specific case. In addition, the cause leading to the deviation between pore-scale modeling and laboratory experiment is also explained. Lastly, several challenges for future research directions are presented.

2. Laboratory experiments for dynamic capillarity effect

In laboratory, flow experiments are better performed by changing boundary conditions monotonically since such changes prevent the occurrence of hysteresis interference (Sakaki et al., 2010). In addition, packed soils in laboratory can reduce the complications that might arise from soil heterogeneity. Meanwhile, noise of surrounding environment can be minimized, which improves the accuracy of measurement data (Diamantopoulos and Durner, 2012). As demonstrated by Lo et al. (2017), acoustic excitation results in a change in contact angle and air-entry pressure, thus affecting the dynamic capillarity effect in sample column. However, experimental approach is time and cost consuming. Meanwhile, laboratory experiments are difficult to determine some micro-scale parameters, such as interface tension and wettability. Additionally, the deviation in experiment is unavoidable owing to manual operation errors.

The schematic of the experimental apparatus is shown in Fig. 2. Along the vertical direction of pressure cell, a set of probes consisting of one non-wetting phase tensiometer (P_{nw}), one wetting phase tensiometer (P_w), and one moisture probe (S_w) are installed at different depths. The local values of P_{nw}, P_w and S_w are then measured at different depths. To up-scale these local values to the core-scale, an averaging process is needed. The conventional way of averaging is expressed below:

$$P_c^c|_{t_n} = \left(\frac{\sum_{j=1}^{m} (1 - S_{wj})\, P_{nwj}}{\sum_{j=1}^{m} (1 - S_{wj})} - \frac{\sum_{j=1}^{m} S_{wj}\, P_{wj}}{\sum_{j=1}^{m} S_{wj}} \right) \Bigg|_{t_n} \tag{2}$$

where $P_c^c|_{t_n}$ represents the core representative capillary pressure at a specific saturation and experimental time, t_n denotes the time at nth count of data generated, $j = 1, 2, \ldots, m$, with m being the total number of measurement depths in the whole sample column. Next, dynamic capillary coefficient can be determined by:

$$P_c^d(S_w) - P_c^s(S_w) = \tau \frac{\partial S_w}{\partial t}(S_w) \tag{3}$$

where P_c^d refers to the dynamic capillary pressure (the instantaneous local pressure difference between the two phases), P_c^s signifies the static capillary pressure (P_c in a static displacement). Thus, P_c^d–S_w, P_c^s–S_w and $\partial S_w/\partial t$–S_w curves are required to obtain the value of τ.

To determine the P_c–S_w curves, a filter system should be equipped with a tensiometer. Such a choice is based on two considerations. On the one hand, the filter system prevents the microparticles in porous media from transporting to the tensiometer. On the other hand, it allows the tensiometer to contact with one fluid solely, thus determining the pressure of each phase, respectively. A common filter system is shown in Fig. 3 (Oung et al., 2005), whose core component is a semi-permeable membrane (hydrophilic or hydrophobic). The membrane is too thin, where a filter plate is required to support it. One of the major drawbacks of this filter system is the limitation of applied pressure (<0.1 MPa). To assess this issue, a tensiometer is developed by connecting ceramic porous cup to pressure transducer (Camps-Roach et al., 2010), however, this arrangement may damage the structure of the porous medium.

To determine the P_c–S_w curves more rapidly, the sample column is always placed between the hydrophobic and hydrophilic membranes (Topp et al., 1967; Kalaydjian, 1992; Sakaki et al., 2010). Nevertheless, several studies have speculated that membrane may

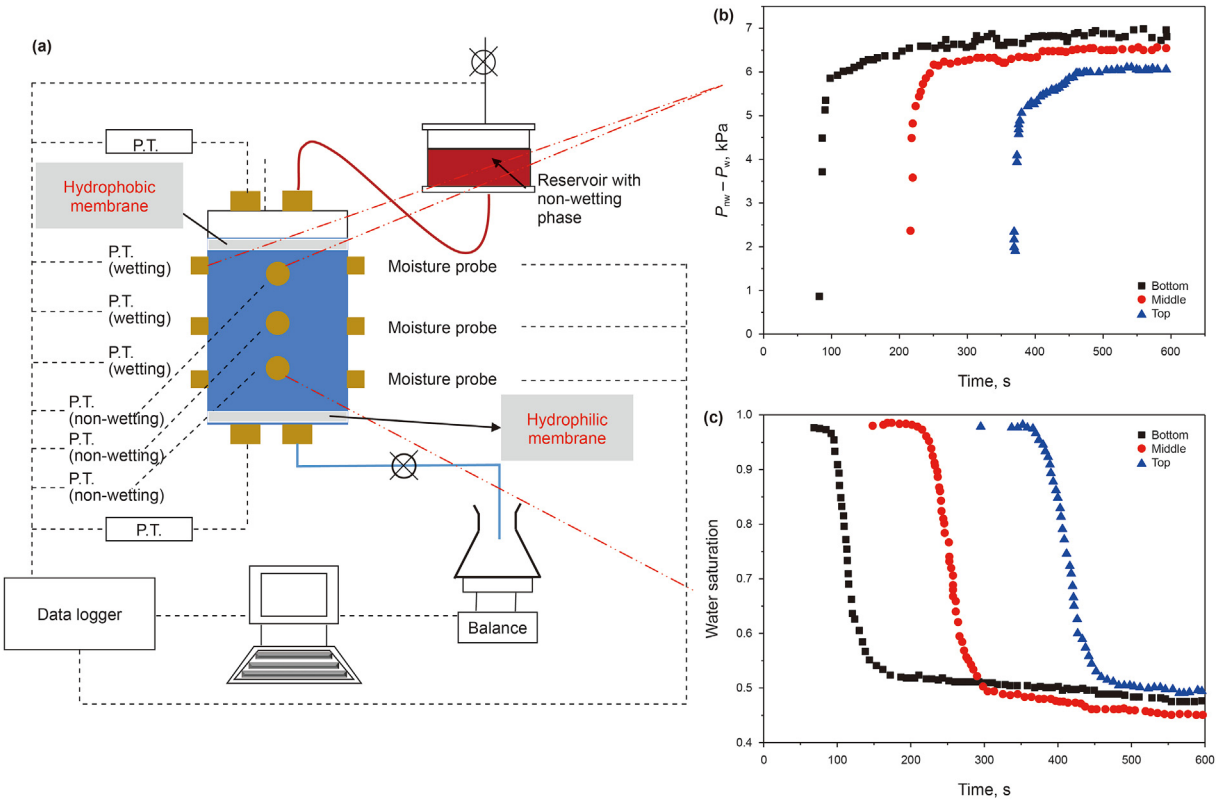

Fig. 2. (**a**) A schematic of experimental set up (Goel and O'Carroll, 2011), wetting phase saturation and pressure difference of two-phase are mainly measured; (**b**) The measured pressure difference of non-wetting and wetting phases at different depths through pressure transducers (Bottero et al. 2011); (**c**) The measured water saturation at different depths through water probe (Bottero et al., 2011). P.T. refers to the pressure transducer.

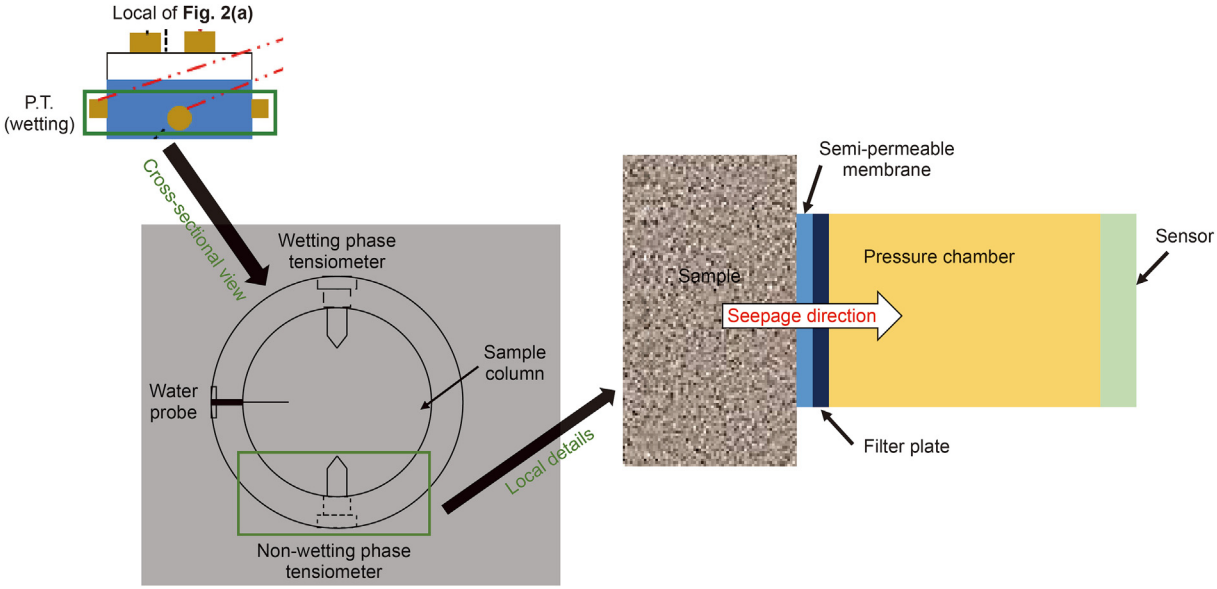

Fig. 3. The illustration of filter system in experimental set up (Camps-Roach et al., 2010; Li, 2018).

obviously affect P_c—S_w curves through disturbing the fluid distribution (Hassanizadeh et al., 2002; Bottero et al., 2006; Goel et al., 2016). In this regard, Li et al. (2020a) designed a special pressure measurement system, including semi-permeable metal plates and pressure transducers, on both sides of the sample. When compared with the traditional semi-permeable plates in Fig. 3, these metal plates have several flow channels in both radius and tangent directions, which ensure fluid to flow evenly. Thus, the disturbance to flow that resulted from filter system can be eliminated. In addition, the maximum test pressure of this special system can reach up to 1000 psi. It is therefore able to study the dynamic flow in low permeability reservoirs.

Table 1
Experimental studies dealing with dynamic capillary effect.

Reference	Length, cm	Fluid	Media	τ, Pa·s	Permeability, m^2
Oung et al. (2005)	18	Water and PCE	Fine sand	$0–8 \times 10^3$	5.7×10^{-5} 3×10^{-5}
Camps-Roach et al. (2010)	20	Air and water	Sand	$1 \times 10^5–6.7 \times 10^5$	1.47×10^{-11} 5.3×10^{-11}
Goel and O'Carroll (2011)	20	Oil and water	Sand	$4.85 \times 10^5–2.74 \times 10^6$	1.47×10^{-11}
O'Carroll et al. (2005)	9.6	Water and PCE	Sand	5.64×10^7	1.58×10^{-11}
Zhuang et al. (2017)	3	Air and water	Sand	$1 \times 10^5–1 \times 10^7$	1.7×10^{-11}
Abidoye and Das (2014b)	4 8 12	Oil and water	Sand	$1.72 \times 10^5–9.08 \times 10^6$ $4.01 \times 10^5–1.31 \times 10^6$ $1.08 \times 10^7–1.25 \times 10^7$	5.66×10^{-11}
Goel et al. (2016)	8 12	Oil and water	Sand	$4.2 \times 10^5–1.3 \times 10^6$ $6.2 \times 10^5–1.82 \times 10^6$	5.66×10^{-11}
Hou et al. (2012)	1.27	Gas and water	Fine sand	$0–10^3$	2.27×10^{-12} 1.88×10^{-10}
Zhang et al. (2015)	–	Standard brine and kerosene	Rock	$3.14 \times 10^{11}–6.10 \times 10^{13}$	$0.33–1.22 \times 10^{-16}$
Tian et al. (2012)	20	Oil and water	Rock	7.92×10^6	2×10^{-16}
Li et al. (2020c)	4	Oil and water	Rock	$1 \times 10^{10}–5 \times 10^{11}$	$1.9–7.1 \times 10^{-16}$
Topp et al. (1967)	7.6	Gas and water	Fine sand	2×10^7	–
Sakaki et al. (2010)	2.9	Water and PCE	Fine sand	$5 \times 10^5–1 \times 10^7$	–
Bottero et al. (2011)	18	Water and PCE	Sand	$1.5 \times 10^6–2.5 \times 10^6$	–
Lo et al. (2017)	100	Air and water	Sand	$0–4 \times 10^5$	–

Note: PCE refers to the perchloroethylene.

Table 1 summarizes various experiments concerning the dynamic capillary effect in two-phase flow. To sum up, there are mainly three deficiencies in the existing experiments. Firstly, sandy soils are selected in the majority of experiments. Whether the dynamic capillary effect is more significant in sandy materials when compared with clay soils? Nonetheless, none of investigations have confirmed that dynamic capillary pressure has ignorable differences with the static one in clay soils (Diamantopoulos and Durner, 2012). Secondly, the length scale of sample column is limited ($\leq$100 cm). In most cases, the length scale is below 20 cm (Table 1). Although various upscaling methods are proposed, it is still difficult to reach the field scale. Lastly, few experiments are conducted on low-permeability reservoir rocks. As shown in Fig. 4, dynamic capillary effect is more significant in lower permeability reservoirs due to their small pore throats. Thus, excellent pressure resistance of experimental apparatus is required to apply higher injection pressure for injecting fluid into these small pore throats.

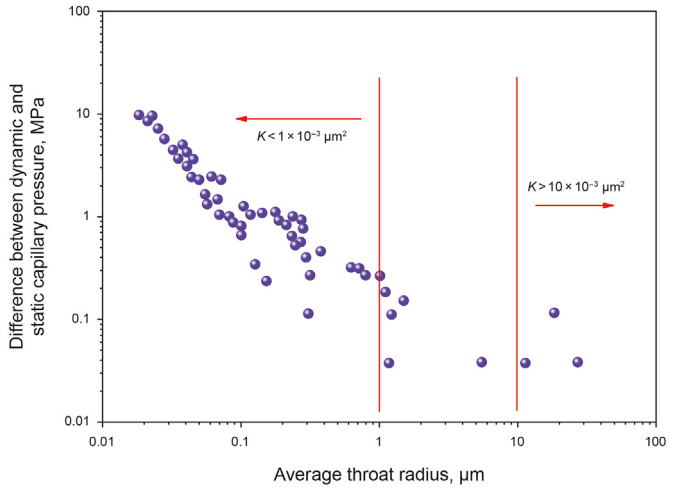

Fig. 4. The difference between dynamic and static capillary pressure with different permeabilities K: high-permeability reservoir, medium-high permeability reservoir, low-permeability reservoir (Zhang et al., 2015).

3. Modeling

3.1. Pore-scale model

Pore-scale models are generally categorized by two types: (i) models that divide the pore space into pore bodies and throats, such as PNMs (Thompson, 2002; Joekar-Niasar et al., 2010; Qin, 2015; Xu et al., 2022) and pore-unit assembly models (Mason and Mellor, 1995) and (ii) models that employ fully resolved simulations of flow within the pore geometry (i.e., direct simulation methods), such as LBM (Vogel et al., 2005), smooth particle hydrodynamics (Tartakovsky and Meakin, 2006; Kunz et al., 2016), computational fluid dynamic simulations (Ferrari and Lunati, 2012; Rabbani et al., 2017), dissipative particle dynamics method (Groot and Warren, 1997), bundle-of-tubes model (Dahle et al., 2005), and volume of fluid method (Raeini et al., 2014a, 2014b). Among them, PNM, LBM, and pore-unit assembly models have been widely performed to investigate the dynamic effect in two-phase flow. Pore-scale model achieves outstanding advances in high-performance computing. Moreover, the accomplishment of pore-scale model requires a comprehensive acquaintance of the morphology of pore geometry and the physical processes at the pore-scale.

3.1.1. LBM

LBM simulates the fluid through virtual particles, which can continuously transmit and collide in discrete lattice mesh (Zhang, 2011). It includes the color-gradient model (Gunstensen et al., 1991; Ba et al., 2016; Liu et al., 2020), the Shan-Chen model (also called the pseudo-potential model) (Shan and Chen, 1993; Jiang and Xu, 2021; Zheng et al., 2021), the free-energy model (Swift et al., 1996), and the mean-field model (He et al., 1999). Among them, the Shan-Chen model has advantages of simplicity, flexibility, and clear description of the basic microscopic physics of phase segregation, which is a favorable alternative to investigate the dynamic capillary effect in two-phase flow.

The basic idea of the Shan-Chen model is to utilize a pseudo-potential that depends on local density and interaction strength to represent the pair-wise microscopic molecular interactions at mesoscopic scale (Huang et al., 2007). Yan et al. (2018) first established a Shan-Chen model to investigate the dynamic effect of two-

phase flow in two-dimensional (2D) porous media. In their work, the D2Q9 lattice cell was selected, then a package of the circular disk was filled into a 500 × 500 square lattice domain to simulate the two-phase flow (Fig. 5). This operation was performed to replicate the displacement phenomenon in two-phase flow.

When the simulation initiates, fluids will invade into the pore space under the action of pressure boundary between top and bottom until the equilibrium is reached. Then, P_c, two-phase saturation (S_w, S_{nw}), and interfacial area (a_{nw}) of the two-phase meniscus at the end of each time interval are obtained. Subsequently, the static or dynamic P_c–S_w/S_{nw}–a_{nw} can be extracted from equilibrium and non-equilibrium flow conditions. On this basis, they manifested that the variation of P_c^d and a_{nw} both increase with larger pressure boundary during a non-equilibrium process. Although this model is relatively simple, it still arouses interest in applying the Shan-Chen model to study the dynamic flow. The deficiency is that the dynamic capillary effect was not quantified by τ.

To fill this knowledge gap, Tang et al. (2018) established a D3Q27 model to investigate the value of τ. Such a choice is based on two considerations. On the one hand, the D3Q19 model is not coincident with the Galilean invariance (Kang and Hassan, 2013). On the other hand, the Reynolds stresses will occur in both D3Q19 and D3Q15 models while this problem can be ignored in the D3Q27 model (Kuwata and Suga, 2015).

According to Eq. (3), a dynamic P_c–S_w curve, a static P_c–S_w curve and $\partial S_w/\partial t$ are required to calculate the value of τ. To obtain the static P_c–S_w curve, simulations with ultra-low flux rates are needed, which consume considerable computational resources. Therefore, Tang et al. (2018) modified Eq. (3) as follows:

$$P_c^{d1}(S_w) - P_c^{s}(S_w) = \tau \frac{\partial S_w^1}{\partial t}(S_w) \tag{4}$$

$$P_c^{d2}(S_w) - P_c^{s}(S_w) = \tau \frac{\partial S_w^2}{\partial t}(S_w) \tag{5}$$

By subtracting Eq. (5) from Eq. (4), the static term can be removed, which yields:

$$P_c^{d2}(S_w) - P_c^{d1}(S_w) = \tau \left(\frac{\partial S_w^2}{\partial t}(S_w) - \frac{\partial S_w^1}{\partial t}(S_w) \right) \tag{6}$$

After finishing the simulation, the resulting P_c in each lattice cell is at the micro-scale. When the dynamic capillary effect at the Darcy-scale is discussed, an upscaling method is required. In this aspect, Tang et al. (2019) presented an explicit definition of P_c^d at the Darcy-scale based on the energy conservation law:

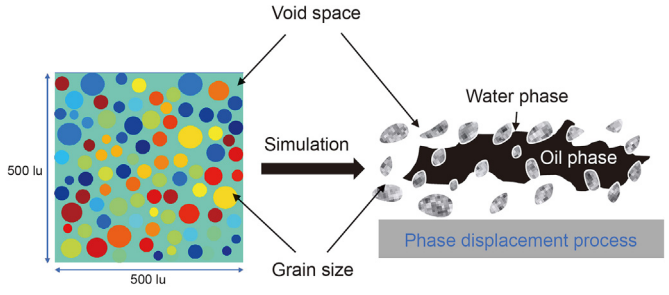

Fig. 5. A package of the circular disk in 500 × 500 lu^2 2D lattice domain (Yan et al., 2018): the various disks represent the soil particles, and the green background denotes the pore space.

$$P_c^d = \frac{dW_p^e - dW_v - dE_k}{q dt} \quad (Q \neq 0) \tag{7}$$

where q is the flow rate. The input energy induced by external pressure (W_p^e) is dispersed on the viscous force (W_V), kinetic (E_k), and P_c. Taking contact angle into account, they performed simulation under 105° and 140°, respectively. They found more wetting phase remained under large contact angles. With larger contact angle, dynamic capillary pressure increases and the change rate of saturation decreases, thus leading to a larger τ.

Likewise, Cao et al. (2020) simulated the dynamic two-phase flow in tight sandstone by constructing a D3Q27 model. Tang et al. (2018) applied the machine learning method to extract pore information, while Cao et al. (2020) adopted the U-net model. Comparing with the machine learning method, the U-net model can record the 3D representation parameters of all pores, and take both the gray threshold and topological structure of the pore space into account. Therefore, the U-net model can greatly improve the accuracy of pore structure characterization, which contributes to simulate the two-phase flow more reliably.

When compared with other pore-scale approaches, LBM can be implemented easily for performing parallel computation (Liu et al., 2012). Meanwhile, it could recover the incompressible Navier-Stokes equation when the fluid velocity is much lower than the sound speed (He and Luo, 1997; Dellar, 2003). More importantly, LBM can solve equations corresponding to arbitrary-complex pore geometry without simplification. Thus, it represents an actual entire porous medium.

3.1.2. Pore network model

In 1985, Koplik and Lasseter (1985) established the first dynamic PNM to simulate dynamic flow of the imbibition process. Since then, great attention has been paid to simulate two-phase flow (drainage and imbibition processes) through the dynamic PNM. Generally, the research process can be summarized as four steps (Gielen et al., 2004, 2005; Joekar-Niasar et al., 2010; Joekar-Niasar and Hassanizadeh, 2011):

(i) Establishing the PNMs to simulate porous media. Note that, the construction of network should be based on the connectivity, shape, and aspect ratio of real pores.
(ii) Solving the local-scale variables (P_c and S_w). The local capillary pressure p_c^i is expressed as:

$$p_c^i = p_{nw}^i - p_w^i = f\left(s_w^i\right) \tag{8}$$

where p_{nw}^i and p_w^i represent the local pressure of non-wetting and wetting phases in pore body i, respectively. s_w^i denotes the local saturation of wetting phase in pore body i.

s_w^i is calculated from the continuity equations, which are written as:

$$\sum_{j=1}^{N_i} \left(Q_{ij}^{nw} + Q_{ij}^{w} \right) = 0 \tag{9}$$

$$V_i \frac{\Delta s_\alpha^i}{\Delta t} = -\sum_{j=1}^{N_i} Q_{ij}^{\alpha}, \quad \alpha = w, nw \tag{10}$$

where V_i refers to the volume; N_i is the set of pore throats connected to the pore body i, Q_{ij}^{nw} and Q_{ij}^{w} designate the non-wetting and wetting phase flux from the pore body i to j, which are

expressed as:

$$Q_{ij}^{\alpha} = \mathbf{K}_{ij}^{\alpha}\left(p_{\alpha}^{j} - p_{\alpha}^{i}\right), \quad (\alpha = \mathrm{w}, \mathrm{nw}) \tag{11}$$

$$\mathbf{K}_{ij}^{\alpha} = \frac{\pi R_{ij}^{4}}{8\mu^{\alpha} L_{ij}}, \ (\alpha = \mathrm{w}, \mathrm{nw}) \tag{12}$$

where $\mathbf{K}_{ij}^{\mathrm{nw}}$ and $\mathbf{K}_{ij}^{\mathrm{w}}$ stand for the non-wetting and wetting phase conductivity from the pore body i to j. R_{ij} and L_{ij} represent the radius and length, respectively.

(iii) Averaging the local-scale variables to the macro-scale,

$$\begin{cases} S_{\mathrm{w}} = \dfrac{V_{\mathrm{w}}}{V_{\mathrm{w}} + V_{\mathrm{nw}}} = \dfrac{\sum_{i=1}^{N} s_{\mathrm{w}}^{i} V_i}{\sum_{i=1}^{N} V_i} \\ S_{\mathrm{nw}} = 1 - S_{\mathrm{w}} \end{cases} \tag{13}$$

$$P_{\mathrm{c}} = \frac{\sum_{i=1}^{N} p_{\mathrm{c}}^{i} A_i}{\sum_{i=1}^{N} A_i} \tag{14}$$

where N is the total number of the pore bodies, V_{w} and V_{nw} denote the volume of wetting and non-wetting phases, V_i is the volume of pore body i, A_i represents the interfacial area between the wetting and non-wetting phases in pore body i.

(iv) Calculating the value of τ from Eq. (3).

Table 2 summarizes the studies of the dynamic capillary effect from different PNMs. The PNMs established by Gielen et al. (2005) have poor simulation results and strong instability under the condition of very small capillary numbers. Meanwhile, many physical processes such as snap-off, capillary diffusion, and local countercurrent flow could not be observed in these simulations. To avoid this, Joekar-Niasar et al. (2010) presented three improvement points: a) allocating two separate pressure fields to the two fluids, so the p_{c}^{i} of each pore body was considered; b) considering the pore-scale flow mechanisms (i.e., snap-off and cooperative pore filling); c) updating saturation by semi-implicit method to enhance the simulation stability at low flow rates. However, their results were only suitable for the drainage process. Subsequently, Joekar-Niasar and Hassanizadeh (2011) discussed the dynamic capillary effect of two-phase flow under both drainage and imbibition processes. Meanwhile, they could simulate a larger pore space by adopting the truncated octahedrons as pore bodies.

PNM has been mainly utilized to investigate the influence of various parameters on two-phase flow. It can easily obtain some variables that are difficult to determine from the experiments. In contrast to LBM, PNM simplifies the pore geometry of real porous media, which obviously reduces computational effort and simulates a much larger domain (Golparvar et al., 2018). Synchronously, this simplification will lead to the omit of pore structure information. Another ubiquitous deficiency of PNM is that the pore geometry of porous medium is assumed to be rigid, regardless of the deformable characteristic of pore geometry and the frequent occurrence of coupled flow in porous media.

3.1.3. Pore-unit assembly model

In the pore-unit assembly model, a pore unit is surrounded by the tetrahedron, whose zeniths are formed by four interfacing spherical particles. The pore geometry of spherical particles is abstracted by regular triangulation. The whole pore space is represented by the assembly of pore units (Mason and Mellor, 1995). A large number of researches reveal that the pore-unit assembly model can be applied to the P_{c}–S_{w} curve in porous media (Gladkikh and Bryant, 2005). Subsequently, some efforts have been devoted to investigate the dynamic capillary effect in two-phase flow. In this regard, Sweijen et al. (2018) simulated dynamic drainage in the packing of spheres by coupling a pore-unit assembly model with the discrete element method. The effectiveness of this model was verified by the quasi-static P_{c}–S_{w} curve. In their work, they analyzed the effect of averaging, boundary condition, domain size, and permeability on the dynamic capillary effect. The results were thereby compared with existing experimental results.

Similar to the PNM, the pore-unit assembly model also simplifies the pore geometry. However, the combination of the discrete element method and the pore-unit assembly model can successfully incorporate the deformation and coupling flow (Yuan et al., 2016).

3.2. Pore-scale flow behavior

3.2.1. Capillary valve effect

Porous media always include substantial pores with different sizes. Large pores are connected by small throats, thus forming a sudden geometrical expansion along pore-throat interface. This expansion will impede the movement of invading fluid. At expansion interface, invading fluid will remain stagnant until the interface pressure difference exceeds a threshold value P_{t}, which is called the “capillary valve effect”.

Due to the capillary valve effect, there are two types of invasion pattern, namely bursting and merging invasion. Bursting invasion occurs when invading fluid advances from a throat to a pore. The threshold value for bursting invasion is written as (Wu et al., 2016a):

$$P_{\mathrm{t}} = 2\sigma\left(\frac{\sin[\max(90^{\circ}, \theta_{\mathrm{a}})]}{\Phi} + \frac{\cos\theta_{\mathrm{a}}}{h}\right) \tag{15}$$

where σ is the surface tension coefficient, θ_{a} represents the advancing contact angle, Φ and h are the width and height of microchannel, respectively. Merging invasion occurs when invading fluid enters a pore from two throats. In this case, menisci at two neighboring throats are merged, thus forming a new meniscus in a pore. The threshold value for merging invasion is calculated as:

$$P_{\mathrm{t}} = \sigma\left(\frac{1}{R} + \frac{2\cos\theta_{\mathrm{a}}}{h}\right) \tag{16}$$

where R is the curvature radius of new meniscus in a pore.

3.2.2. Snap-off

During imbibition process, two-phase fluid interfaces at corners will become unstable when local capillary pressure in a pore throat p_{c}^{ij} is smaller than a critical value, and thus leading to the occurrence of fluid snap-off. As for square cross-sectional pore throat, Vidales et al. (1998) proposed a criterion:

$$p_{\mathrm{c}}^{ij} \le \frac{\sigma}{R_{ij}}(\cos\theta - \sin\theta) \tag{17}$$

It is always assumed that as soon as snap-off appears, wetting

Table 2
The summary of the literature for PNMs.

Reference	Pore body/throat	Basic assumption*	Domain size (width/length/height), cm	K, 10^{-12} m^2	Process	τ, Pa·s
Gienlen et al. (2005)	Spherical/cylinder	Local capillary pressure is zero	0.3/0.3/1	–	Drainage	5×10^3 -4×10^4
Joekar-Niasar et al. (2010)	Cubic/square	Local capillary pressure is considered.	0.5/0.5/0.5	150	Drainage	10^2–10^4
Joekar-Niasar and Hassanizadeh (2011)	Truncated octahedrons/parallelepiped	Local capillary pressure is considered.	0.19/0.19/0.19	1.43	Drainage imbibition	10^2–10^4

Note: * Gravity is neglected, and flow in the pore throats is laminar.

phase fully occupies pore throat, and the nonwetting phase immediately retreats into the two neighboring pore bodies.

Both capillary valve effect and snap-off will greatly affect interface shape and interface force, and in turn altering the P_c. Theoretically, these pore-scale flow behavior also have influence on the dynamic capillary effect. In this aspect, Wu et al. (2016b) demonstrated that flow pattern is capillary fingering when bursting invasion is dominated, while it is stable when merging invasion is dominated. Xu et al. (2017) presented a LBM color-gradient model to study the dynamic constant angle, indicating that the difference in threshold pressure is the origin of preferential flow paths due to the capillary valve effect. Hence, qualitatively discussing the effect of capillary valve effect and snap-off on the dynamic capillary effect is proposed to be the focus for future research.

3.3. Macro-scale models

3.3.1. Stauffer model

To describe the dynamic P_c–S_w relationship, Stauffer (1978) replaced the static P_c by dynamic one in the Brooks and Corey (1964) model. Based on experimental observations, the dynamic capillary effect is described as:

$$\tau=\frac{\alpha\phi\mu_w}{\lambda k}\left(\frac{P^d}{\rho_w g}\right)^2 \tag{18}$$

where α is a constant ($\alpha=0.1$), ϕ designates the porosity, P^d stands for the entry pressure, λ denotes the pore size distribution index, μ_w reflects the viscosity of the wetting phase, k represents the intrinsic permeability, g and ρ_w are the gravity constant and the density of wetting phase, respectively. In Eq. (18), τ is defined by the properties of fluids (μ_w, ρ_w) and porous media (ϕ, λ, k, P^d). Since these properties are considered constant, the value of τ in Eq. (18) is also regarded as constant in laboratory. Gielen (2007) stated that $P^d/\rho_w g$ is defined as a characteristic length scale L_s of the porous medium. Then they found τ varies linearly with μ_w and L_s.

In Eq. (18), the contribution of non-wetting phase properties on the dynamic capillary effect is neglected, regardless of the significant influence of these properties on two-phase flow (Hassanizadeh and Gray, 1993; Das et al., 2007; Joekar-Niasar and Hassanizadeh, 2011; Hou et al., 2014). In addition, no dependence on saturation is included. Subsequently, Joekar-Niasar and Hassanizadeh (2011) modified Eq. (18) by incorporating an effective viscosity μ_{eff}:

$$\mu_{eff}=\mu_{nw}S_{nw}+\mu_w S_w \tag{19}$$

$$\tau=\frac{\alpha\phi\mu_{eff}}{\lambda k}\left(\frac{P^d}{\rho_w g}\right)^2 \tag{20}$$

where μ_{nw} is the viscosity of non-wetting phase, μ_{eff} depends on the fluid viscosities and spatial fluid distribution, which is linearly weighted by saturation. Eq. (20) is only valid for the case where a piston-like movement is dominated.

3.3.2. Hassanizadeh and Gray model

As shown in Eq. (3), Hassanizadeh and Gray (1993) proposed a thermodynamically-based relationship between P_c^d and P_c^s. For a drainage process, the rate of desaturation ($\partial S_w/\partial t$) is negative. Thus, the P_c^s is smaller than P_c^d. The opposite is true for the wetting process. The relationship between ($P_c^d-P_c^s$) and $\partial S_w/\partial t$ is a straight line with a slope of τ. When $\partial S_w/\partial t$ is zero, Eq. (3) is simplified to Eq. (1).

Eq. (3) has been the subject of several previous studies, computationally using the Darcy-scale models (Manthey et al., 2005; Das et al., 2006) and the pore-scale models (Joekar-Niasar et al., 2010; Joekar-Niasar and Hassanizadeh, 2011) as well as experiments (Oung et al., 2005; Bottero et al., 2006; Camps-Roach et al., 2010). Strictly, dynamic effect includes the dynamic capillary effect and the relative permeability effect, but only the dynamic phenomenon in P_c–S_w relationship is involved in Eq. (3).

3.3.3. Barenblatt model

Taking the relative permeability effect and the dynamic capillary effect both into account, Barenblatt (1971) assumed that dynamic relative permeability (k_r^d) and P_c^d can be expressed by their static counterparts at a certain situation:

$$\begin{aligned} k_{rw}^d(S_w)&=k_{rw}^s(S_{ew})\\ k_{ro}^d(S_w)&=k_{ro}^s(S_{ew})\\ P_c^d(S_w)&=P_c^s(S_{ew}) \end{aligned} \tag{21}$$

where k_{rw}^d, k_{rw}^s denote the dynamic and static relative permeability of the water phase, k_{ro}^d, k_{ro}^s reflect the dynamic and static relative permeability of the oil phase, S_{ew} is the effective water saturation. A relationship between the actual saturation S_w and effective saturation S_{ew} is demanded to apply Eq. (21):

$$S_{ew}=S_w+\tau_B(S_w)\frac{\partial S_w}{\partial t} \tag{22}$$

where τ_B represents the relaxation time, which is defined as the time to reach an equilibrium of fluids in porous media. As stated by Barenblatt et al. (2002), dynamic capillary effect is caused by the redistribution processes at the pore-scale. At the equilibrium state, S_{ew} is equal to S_w.

Subsequently, Juanes (2008) found that the relationship

between τ and τ_B is written as:

$$\tau(S_w) = \left|\frac{dP_c^s}{dS_w}\right| \tau_B(S_w) \tag{23}$$

From the perspective of pore-scale, it concludes that the dynamic capillary effect should be ignored for the slow flow processes whose time scale is in the order of τ_B. However, it must be considered for the fast flow processes whose time scale is smaller than τ_B (Barenblatt et al., 2002).

3.3.4. Das model

To consider the lumped effects of various fluid properties, Das et al. (2007) proposed a model to describe the relationship between τ and flow direction, viscosity as well as density ratio:

$$\tau = C\frac{P^d V^{1/6}}{\sqrt{g}}\left(\frac{\phi}{\lambda}\times\frac{\rho_{nw}\mu_w}{\rho_w\mu_{nw}}\right)^a\left(\frac{k}{V^{2/3}}\right)^b (S_w)^c \tag{24}$$

where V is the domain scale, ρ_{nw} denotes the fluid density of the non-wetting phase, C represents a dimensionless constant of proportionality, $a = f(k/V^{2/3})$, $b = f(S_w)$, and c are the dimensionless coefficients. In Eq. (24), a scaling relationship is found, indicating that τ varies with S_w and V. The reliability of Eq. (24) was demonstrated by numerical results, but its applicability on heterogeneous domains needs further studies. Targeting different scenarios, the values of C, a, b, c are different.

3.3.5. Abidoye and Das model

Based on the Buckingham's G-theorem, Abidoye and Das (2014b) determined sets of dimensionless parameters from chosen variables. Then, two dimensionless groups of variables were demanded to describe the combined effect of various variables on τ:

$$\begin{cases} \Pi_1 = \dfrac{\tau\sqrt{g}}{k^{1/4}P^d} \\ \Pi_2 = \dfrac{Vk^{\frac{-3}{2}}}{\phi\lambda S_w}\dfrac{\rho_{nw}\mu_{nw}}{\rho_w\mu_w} \end{cases} \tag{25}$$

According to the non-linear form of $\Pi_1 = a[\Pi_3]^b$, the dynamic capillary effect model can be written as:

$$\frac{\tau\sqrt{g}}{k^{1/4}P^d} = a\left[\frac{Vk^{\frac{-3}{2}}}{\phi\lambda S_w}\frac{\rho_{nw}\mu_{nw}}{\rho_w\mu_w}\right]^b \tag{26}$$

This approach has the advantage that it is possible to find out how many dimensionless groups are required to replace the variables, which affects the dynamic capillary effect.

3.3.6. Civan model

Taking the temperature into account, Civan (2012) considered that τ is a function of irreducible wetting-phase saturation, which depends on temperature:

$$\tau = \frac{\mu_w(1-S_{nwi}-S_{wi})^{a_1}}{2E_{nw}^o\vartheta(S_w-S_{wi})^{b_1}}, \quad a_1, b_1 > 0 \tag{27}$$

where S_{wi}, S_{nwi} are the irreducible saturation of wetting and non-wetting phases, E_{nw}^o denotes the empirical coefficient; ϑ represents a rate coefficient, a_1, b_1 are the empirical fitting parameters. Among them, a_1, b_1, S_{wi}, and S_{nwi} are dependent on temperature. As shown in Fig. 6, a linear relationship is found between the scaled parameters and temperature. To be more specific, b_1 and S_{wi} increase with an increasing temperature, while a_1 decreases as temperature increases.

3.3.7. Li model

Considering the effect of fracture, Li et al. (2020b) confirmed the existence of fracture leads to a decrease of pressure imposing area (Fig. 7), thus weakening the dynamic capillary effect. Then, dynamic capillary effect of fractured rocks can be expressed as:

$$\tau = \omega(S_w)^{b_2}\frac{L_c^2}{k}P^d\sqrt{\frac{L_c}{g}} \tag{28}$$

$$L_c = \frac{V}{A_c} = \frac{V}{A_1+A_2+A_3} = \frac{\pi R^2 L}{\pi R^2 + 4RL\phi_f} = L - \frac{4L^2\phi_f}{\pi R + 4L\phi_f} \tag{29}$$

$$\omega = \eta\frac{\phi\rho_w\mu_{eff}}{\lambda\rho_{nw}\mu_w} \tag{30}$$

where ω, η, and b_2 are the fitting parameters, ϕ_f is the fracture porosity, L_c means the effective pressure imposing length, L denotes the rock length, R signifies the rock radius, A_c is the pressure imposing area. Note that, the orientation, aperture, and other properties of fracture also influence the dynamic capillary effect. Thus, further studies are demanded to establish the dynamic capillary coefficient models, which incorporate the lumped effects of various properties of fracture.

3.4. Upscaling from pore- to Darcy-scale

P_c is a pore-scale phenomenon, and refers to the pressure difference across the two-phase fluid interface at the static state:

$$P_c = P_{nw} - P_w \tag{31}$$

In a porous medium, it is more difficult to measure P_c at the pore-scale owing to the more complicated internal construction (Ferrari and Lunati, 2013). Thus, a macro-scale P_c defined in Eq. (1) is proposed. In laboratory experiments, the average macro-scale P_c in Eq. (1) is calculated as the pressure difference between the non-wetting phase at the inlet (P_{in}) and wetting-phase at the outlet (P_{out}). Therefore, Eq. (1) can be rewritten as:

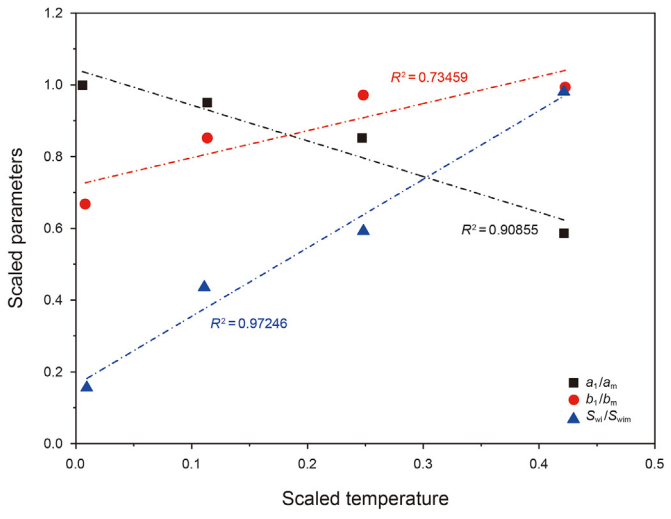

Fig. 6. The relationship between temperature and parameters in Eq. (27) (a_m, b_m, S_{wim} are the maximum values of a_1, b_1, S_{wi}).

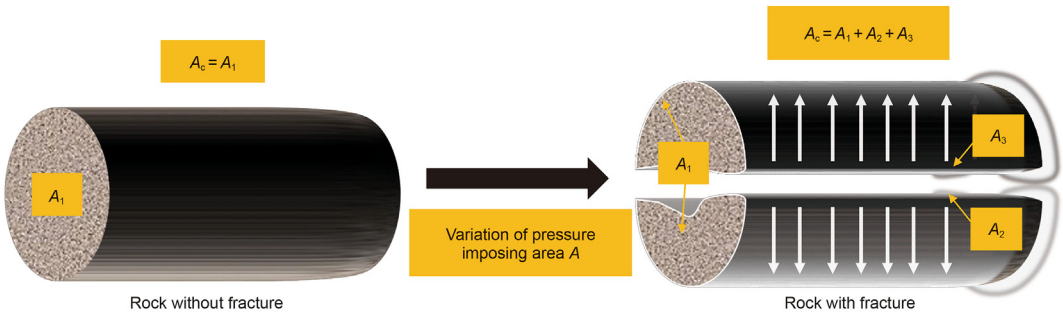

Fig. 7. The variation of pressure imposing area with fracture (Li et al., 2020b).

$$\Delta P^{io} = P_{in} - P_{out} = P_c(S_w) \tag{32}$$

where ΔP^{io} is the total pressure drop across the porous medium between the inlet and outlet. Conventionally, ΔP^{io} is equal to the pore-scale P_c in Eq. (31) under all conditions. However, considerable studies have demonstrated that this is not the case when the fluid pressures within the pores vary with time and space due to the dynamic capillary effect. Under the dynamic flow, macro-scale P_c includes the pore-scale P_c and pressure head caused by the viscous effects:

$$\Delta P^{io} = \Delta P^{in} + P_{vis} \tag{33}$$

where ΔP^{in} represents the pore-scale capillary pressure, P_{vis} is the pressure head caused by the viscous effects. In fact, pore-scale P_c is the "true capillary forces" in porous media, which should be upscaled to obtain the macro-scale P_c–S_w relationship. In laboratory experiments, it is difficult to measure the true capillary forces without accounting for the viscous pressure head. Fortunately, this difficulty can be overcome through the pore-scale simulations.

4. ANN

ANN is a certainly useful modeling tool to extract desired information from data, which can mimic the labor of the human brain and the ability of the nervous system to perform functions. It mainly consists of various "neurons", which are divided into interconnected subsets, including input, hidden and output layers, having respective biases, weights, and transfer functions (Mueller and Hemond, 2013). Then, comprehensive neurons constitute a network, which builds the relationships between the inputs and outputs through transfer functions and controls the values of biases and weights. As for two-phase flow system, the corresponding modeling parameters have complicated relevance, however ANN can guarantee the accuracy of relevant functions (Hanspal et al., 2013). Therefore, it is worth considering that the ability of ANN for predicting the dynamic capillary effect.

This ability was first demonstrated by Hanspal et al. (2013). They found that ANN can describe the relationship between the changes in porous media and fluid properties, so it can predict the dynamic capillary effect in two-phase flow accurately and ensure that τ is a function of water saturation. Unfortunately, the dependency of dynamic capillary effect on domain scale and heterogeneity was ignored. To address these issues, Abidoye and Das (2014a) utilized ANN to investigate the effect of domain scale on τ using the published experimental data, the results show that the magnitude of τ increases as domain size increases. Concerning heterogeneous porous media, Das et al. (2015) developed a new ANN approach to quantify the magnitude of τ in heterogeneous porous media with different heterogeneity intensity w. The simulation results indicate that an increase in w leads to a larger τ.

Most of the experimental and computational flow-physics-based techniques employed to describe and quantify the dynamic capillary effect are very resource-intensive and extremely time-consuming for complex three-dimensional (3D) fluid flows. Surprisingly, ANN is easily and conveniently to be established, so it can obviously reduce the cost and computational time. Meanwhile, studies have further shown that ANN is capable of offering the physically realistic values of τ, which ensures the accuracy of the application of ANN on dynamic two-phase flow. Note that, ANN has great advantages of studying the dynamic capillary effect in heterogeneous domains where experiments and other numerical models are difficult to solve.

5. Discussion

Accurate representation of the P_c–S_w relationship under dynamic two-phase flow is essential for improving the oil recovery in low-permeability reservoirs. Up to date, impressive advances have been made to account for the dynamic capillary effect. As for laboratory experiment, macro-theoretical model, and PNMs, some future directions are summarized as follows:

(1) Dynamic capillary effect is extremely obvious in low-permeability reservoirs, especially for ultra-low permeability reservoirs. Due to the presence of the dynamic capillary effect, the oil recovery of these unconventional reservoirs will greatly reduce. Hence, more experiments should be done for low-permeability reservoirs. Low-permeability reservoirs have the characteristic of small pore throat, hence the required displacement pressure is relatively higher. In this case, the requirements for the filter system are higher. More improved apparatus should be designed to apply the high displacement pressure without destroying the structure of porous media.

(2) P_c at the pore-scale is the pressure difference between the interface between two fluid phases. It represents the "true capillary forces" in the system, which is only related to pore shape and interfacial energy of the two phases. In experiment, final measured P_c at the macro-scale always includes the viscous pressure head. Many studies have demonstrated that macroscopic P_c only agrees well with "true capillary force" at the equilibrium state. However, macro-scale P_c contains the pore-scale P_c at fluid-fluid interface and viscous pressure head at dynamic state.

(3) Inspection of aforementioned macro-models, the value of τ is closely related to the porosity, entry pressure, and permeability, thus it significantly relies on the micro-structure of porous medium. Therefore, an accurate description of

microstructure is beneficial to investigate the dynamic capillary effect more exactly. It is reported that fractal geometry is a prominent approach to represent the pore throat structure and analyze the fluid flow of porous media. Therefore, it is feasible to develop a fractal theoretical model to quantify the dynamic capillary effect.

(4) Up to date, none of the researchers have directly compared the simulation results of pore-scale models with experimental results of two-phase flow. Because it is still challenging to monitor pore-scale real measurements in 3D domains. Once this problem is solved, the simulation results of pore-scale models can be closer to the natural condition. As for PNMs, complex quasi-static PNMs with mixed-cross-sectional pores and unstructured irregular networks have already been developed, while the network structures of dynamic PNMs are still quite simple. This may lead to a deviation in the study of dynamic capillary effect. Therefore, it is required to develop dynamic PNMs with complex pore topology and geometry.

6. Conclusion

The non-equilibrium flow in porous media frequently occurs in petroleum, chemical, and environmental engineering, which leads to a much more complex relationship between capillary pressure and saturation. Thus, the dynamic capillary effect has been a subject of global interest with huge investment and research. This review systematically summarizes various methods to investigate and quantify the dynamic capillarity effect, including laboratory experiments, the macro-scale models, the pore-scale models as well as the artificial neural networks. The evaluation and future development of each method are discussed. Furthermore, a more accurate and easy operating method is anticipated to depict the dynamic capillary effect of two-phase flow.

Acknowledgments

This study was financially supported by the National Natural Science Foundation of China (No. 42102149), and the Fundamental Research Funds for the Central Universities (No. 2462021YXZZ005).

References

Abidoye, L.K., Das, D.B., 2014a. Artificial neural network modeling of scale-dependent dynamic capillary pressure effects in two-phase flow in porous media. J. Hydroinf. 17, 446–461. https://doi.org/10.2166/hydro.2014.079.

Abidoye, L.K., Das, D.B., 2014b. Scale dependent dynamic capillary pressure effect for two-phase flow in porous media. Adv. Water Resour. 74, 212–230. https://doi.org/10.1016/j.advwatres.2014.09.009.

Ansarinasab, J., Jamialahmadi, M., 2016. Investigating the effect of interfacial tension and contact angle on capillary pressure curve, using free energy Lattice Boltzmann method. J. Nat. Gas Sci. Eng. 35, 1146–1157. https://doi.org/10.1016/j.jngse.2016.09.055.

Ba, Y., Liu, H., Li, Q., Kang, Q., Sun, J., 2016. Multiple-relaxation-time color-gradient lattice Boltzmann model for simulating two-phase flows with high density ratio. Phys. Rev. E 94, 023310. https://doi.org/10.1103/PhysRevE.94.023310.

Barenblatt, G.I., 1971. Filtration of two nonmixing fluids in a homogeneous porous medium. Fluid Dynam. 6, 857–864. https://doi.org/10.1007/BF01013869.

Barenblatt, G., Patzek, T., Silin, D., 2002. The mathematical model of non-equilibrium effects in water-oil displacement. In: SPE/DOE Improved Oil Recovery Symposium. https://doi.org/10.2118/75169-MS.

Bear, J., Verruijt, A., 1987. Theory and applications of transport in porous media. In: Crolet, J.M. (Ed.), Computational Methods for Flow and Transport in Porous Media. Springer, Dordrecht.

Bottero, S., Hassanizadeh, S.M., Kleingeld, P., Bezuijen, A., 2006. Experimental study of dynamic capillary pressure effect in two-phase flow in porous media. In: Proceedings of the XVI International Conference on Computational Methods in Water Resources.

Bottero, S., Hassanizadeh, S.M., Kleingeld, P.J., Heimovaara, T.J., 2011. Nonequilibrium capillarity effects in two-phase flow through porous media at different scales. Water Resour. Res. 47, W10505. https://doi.org/10.1029/2011WR010887.

Brooks, R.H., Corey, A.T., 1964. Hydraulic properties of porous media. Hydrol. Pap. 7, 26–28.

Cai, J., Jin, T., Kou, J., Zou, S., Xiao, J., Meng, Q., 2021. Lucas–washburn equation-based modeling of capillary-driven flow in porous systems. Langmuir 37, 1623–1636. https://doi.org/10.1021/acs.langmuir.0c03134.

Cai, J., Perfect, E., Cheng, C.-L., Hu, X., 2014. Generalized modeling of spontaneous imbibition based on Hagen–Poiseuille flow in tortuous capillaries with variably shaped apertures. Langmuir 30, 5142–5151. https://doi.org/10.1021/la5007204.

Cai, J., Yu, B., 2011. A discussion of the effect of tortuosity on the capillary imbibition in porous media. Transp. Porous Media 89, 251–263. https://doi.org/10.1007/s11242-011-9767-0.

Camps-Roach, G., O'Carroll, D.M., Newson, T.A., Sakaki, T., Illangasekare, T.H., 2010. Experimental investigation of dynamic effects in capillary pressure: grain size dependency and upscaling. Water Resour. Res. 46, W08544. https://doi.org/10.1029/2009WR008881.

Cao, Y., Tang, M., Zhang, Q., Tang, J., Lu, S., 2020. Dynamic capillary pressure analysis of tight sandstone based on digital rock model. Capillarity 3, 28–35. https://doi.org/10.46690/capi.2020.02.02.

Chen, Y., Mao, Y., Yang, L., Wei, W., Meng, Q., Cai, J., 2022. A comprehensive review of factors affecting dynamic capillary effect in two-phase flow. Transport Porous Media 1–22. https://doi.org/10.1007/s11242-021-01723-x (in press).

Civan, F., 2012. Temperature dependency of dynamic coefficient for nonequilibrium capillary pressure-saturation relationship. AIChE J. 58, 2282–2285. https://doi.org/10.1002/aic.13817.

Dahle, H.K., Celia, M.A., Hassanizadeh, S.M., 2005. Bundle-of-tubes model for calculating dynamic effects in the capillary-pressure-saturation relationship. Transp. Porous Media 58, 5–22. https://doi.org/10.1007/s11242-004-5466-4.

Das, D.B., Gauldie, R., Mirzaei, M., 2007. Dynamic effects for two-phase flow in porous media: fluid property effects. AIChE J. 53, 2505–2520. https://doi.org/10.1002/aic.11292.

Das, D.B., Mirzaei, M., Widdows, N., 2006. Non-uniqueness in capillary pressure–saturation–relative permeability relationships for two-phase flow in porous media: interplay between intensity and distribution of random micro-heterogeneities. Chem. Eng. Sci. 61, 6786–6803. https://doi.org/10.1016/j.ces.2006.07.028.

Das, D.B., Thirakulchaya, T., Deka, L., Hanspal, N.S., 2015. Artificial neural network to determine dynamic effect in capillary pressure relationship for two-phase flow in porous media with micro-heterogeneities. Environ. Process. 2, 1–18. https://doi.org/10.1007/s40710-014-0045-3.

Dellar, P.J., 2003. Incompressible limits of lattice Boltzmann equations using multiple relaxation times. J. Comput. Phys. 190, 351–370. https://doi.org/10.1016/S0021-9991(03)00279-1.

Diamantopoulos, E., Durner, W., 2012. Dynamic nonequilibrium of water flow in porous media: a review. Vadose Zone J. 11, vzj2011.0197. https://doi.org/10.2136/vzj2011.0197.

Ferrari, A., Lunati, I., 2012. Direct simulation of interface dynamics: linking capillary pressure, interfacial area and surface energy. XIX International Conference on Water Resources.

Ferrari, A., Lunati, I., 2013. Direct numerical simulations of interface dynamics to link capillary pressure and total surface energy. Adv. Water Resour. 57, 19–31. https://doi.org/10.1016/j.advwatres.2013.03.005.

Friedman, S.P., 1999. Dynamic contact angle explanation of flow rate-dependent saturation-pressure relationships during transient liquid flow in unsaturated porous media. J. Adhes. Sci. Technol. 13, 1495–1518. https://doi.org/10.1163/156856199X00613.

Gao, L., Yang, Z., Shi, Y., 2018. Experimental study on spontaneous imbibition characteristics of tight rocks. Adv. Geo-Energy Res. 2, 292–304. https://doi.org/10.26804/ager.2018.03.07.

Gielen, T., Hassanizadeh, S., Celia, M., Dahle, H., Leijnse, A., 2004. A pore-scale network approach to investigate dynamic effects in multiphase flow. Dev. Water Sci. 55, 83–94. https://doi.org/10.1016/S0167-5648(04)80039-X.

Gielen, T., Hassanizadeh, S., Leijnse, A., Nordhaug, H., 2005. Dynamic effects in multiphase flow: a pore-scale network approach. In: Das, D.B., Hassanizadeh, H.S.M. (Eds.), Upscaling Multiphase Flow in Porous Media. Springer, Dordrecht, pp. 217–236.

Gielen, T.W.J., 2007. Dynamic Effect in Two-phase Flow in Porous Media: a Pore-Scale Network Approach. Doctoral Thesis. Delft University of Technology. http://repository.tudelft.nl/assets/uuid:06275687-01ba-4494-b946.

Gladkikh, M., Bryant, S., 2005. Prediction of imbibition in unconsolidated granular materials. J. Colloid Interface Sci. 288, 526–539. https://doi.org/10.1016/j.jcis.2005.03.029.

Goel, G., Abidoye, L.K., Chahar, B.R., Das, D.B., 2016. Scale dependency of dynamic relative permeability–satuartion curves in relation with fluid viscosity and dynamic capillary pressure effect. Environ. Fluid Mech. 16, 945–963. https://doi.org/10.1007/s10652-016-9459-y.

Goel, G., O'Carroll, D.M., 2011. Experimental investigation of nonequilibrium capillarity effects: fluid viscosity effects. Water Resour. Res. 47, W09507. https://doi.org/10.1029/2010WR009861.

Golparvar, A., Zhou, Y., Wu, K., Ma, J., Yu, Z., 2018. A comprehensive review of pore scale modeling methodologies for multiphase flow in porous media. Adv. Geo-Energy Res. 2, 418–440. https://doi.org/10.26804/ager.2018.04.07.

Groot, R.D., Warren, P.B., 1997. Dissipative particle dynamics: bridging the gap between atomistic and mesoscopic simulation. J. Chem. Phys. 107, 4423–4435. https://doi.org/10.1063/1.474784.

Gunstensen, A.K., Rothman, D.H., Zaleski, S., Zanetti, G., 1991. Lattice Boltzmann model of immiscible fluids. Phys. Rev. A 43, 4320–4327. https://doi.org/10.1103/PhysRevA.43.4320.
Hanspal, N.S., Allison, B.A., Deka, L., Das, D.B., 2013. Artificial neural network (ANN) modeling of dynamic effects on two-phase flow in homogenous porous media. J. Hydroinf. 15, 540–554. https://doi.org/10.2166/hydro.2012.119.
Hassanizadeh, S.M., Celia, M.A., Dahle, H.K., 2002. Dynamic effect in the capillary pressure–saturation relationship and its impacts on unsaturated flow. Vadose Zone J. 1, 38–57. https://doi.org/10.2113/1.1.38.
Hassanizadeh, S.M., Gray, W.G., 1993. Thermodynamic basis of capillary pressure in porous media. Water Resour. Res. 29, 3389–3405. https://doi.org/10.1029/93WR01495.
He, X., Chen, S., Zhang, R., 1999. A lattice Boltzmann scheme for incompressible multiphase flow and its application in simulation of Rayleigh–Taylor instability. J. Comput. Phys. 152, 642–663. https://doi.org/10.1006/jcph.1999.6257.
He, X., Luo, L., 1997. Lattice Boltzmann model for the incompressible Navier–Stokes equation. J. Stat. Phys. 88, 927–944. https://doi.org/10.1023/B:JOSS.0000015179.12689.e4.
Hou, L., Chen, L., Kibbey, T.C., 2012. Dynamic capillary effects in a small-volume unsaturated porous medium: implications of sensor response and gas pressure gradients for understanding system dependencies. Water Resour. Res. 48, W11522. https://doi.org/10.1029/2012WR012434.
Hou, L., Sleep, B.E., Kibbey, T.C., 2014. The influence of unavoidable saturation averaging on the experimental measurement of dynamic capillary effects: a numerical simulation study. Adv. Water Resour. 66, 43–51. https://doi.org/10.1016/j.advwatres.2014.01.008.
Huang, H., Thorne Jr., D.T., Schaap, M.G., Sukop, M.C., 2007. Proposed approximation for contact angles in Shan-and-Chen-type multicomponent multiphase lattice Boltzmann models. Phys. Rev. E 76, 066701. https://doi.org/10.1103/PhysRevE.76.066701.
Jiang, M., Xu, Z.G., 2021. Pore-scale investigation on reactive flow in non-uniform dissolved porous media considering immiscible phase by lattice Boltzmann method. J. Nat. Gas Sci. Eng. 96, 104280. https://doi.org/10.1016/j.jngse.2021.104280.
Joekar-Niasar, V., Hassanizadeh, S.M., 2011. Effect of fluids properties on non-equilibrium capillarity effects: dynamic pore-network modeling. Int. J. Multiphase Flow 37, 198–214. https://doi.org/10.1016/j.ijmultiphaseflow.2010.09.007.
Joekar-Niasar, V., Hassanizadeh, S.M., Dahle, H.K., 2010. Non-equilibrium effects in capillarity and interfacial area in two-phase flow: dynamic pore-network modelling. J. Fluid Mech. 655, 38–71. https://doi.org/10.1017/S0022112010000704.
Juanes, R., 2008. Nonequilibrium effects in models of three-phase flow in porous media. Adv. Water Resour. 31, 661–673. https://doi.org/10.1016/j.advwatres.2007.12.005.
Kalaydjian, F.-M., 1992. Dynamic capillary pressure curve for water/oil displacement in porous media: theory vs. experiment. In: SPE Annual Technical Conference and Exhibition. https://doi.org/10.2118/24813-MS.
Kang, S.K., Hassan, Y.A., 2013. The effect of lattice models within the lattice Boltzmann method in the simulation of wall-bounded turbulent flows. J. Comput. Phys. 232, 100–117. https://doi.org/10.1016/j.jcp.2012.07.023.
Koplik, J., Lasseter, T., 1985. Two-phase flow in random network models of porous media. SPE J. 25, 89–100. https://doi.org/10.2118/11014-PA.
Kunz, P., Zarikos, I.M., Karadimitriou, N.K., Huber, M., Nieken, U., Hassanizadeh, S.M., 2016. Study of multi-phase flow in porous media: comparison of SPH simulations with micro-model experiments. Transp. Porous Media 114, 581–600. https://doi.org/10.1007/s11242-015-0599-1.
Kuwata, Y., Suga, K., 2015. Anomaly of the lattice Boltzmann methods in three-dimensional cylindrical flows. J. Comput. Phys. 280, 563–569. https://doi.org/10.1016/j.jcp.2014.10.002.
Li, Y., 2018. Dynamic Capillarity Characteristics and Application during the Waterflooding Process in Low Permeability Oil Reservoirs. Doctoral Thesis. Southwest Petroleum University.
Li, Y., Cui, X., Li, H., Chen, S., Zhang, Q., 2020a. An in-situ capillary pressure measurement method to characterize pore structure of tight formation. J. Petrol. Sci. Eng. 192, 107270. https://doi.org/10.1016/j.petrol.2020.107270.
Li, Y., Li, H., Cai, J., Ma, Q., Zhang, J., 2018. The dynamic effect in capillary pressure during the displacement process in ultra-low permeability sandstone reservoirs. Capillarity 1, 11–18. https://doi.org/10.26804/capi.2018.02.01.
Li, Y., Li, H., Chen, S., Luo, H., Liu, C., 2020b. Investigation of the dynamic capillary pressure during displacement process in fractured tight rocks. AIChE J. 66, e16783. https://doi.org/10.1002/aic.16783.
Li, Y., Liu, C., Li, H., Chen, S., Huang, S., 2020c. A comprehensive modelling investigation of dynamic capillary effect during non-equilibrium flow in tight porous media. J. Hydrol. 584, 124709. https://doi.org/10.1016/j.jhydrol.2020.124709.
Liu, H., Valocchi, A.J., Kang, Q., 2012. Three-dimensional lattice Boltzmann model for immiscible two-phase flow simulations. Phys. Rev. E 85, 046309. https://doi.org/10.1103/PhysRevE.85.046309.
Liu, Y., Cai, J., Sahimi, M., Qin, C., 2020. A study of the role of microfractures in counter-current spontaneous imbibition by lattice Boltzmann simulation. Transp. Porous Media 133, 313–332. https://doi.org/10.1007/s11242-020-01425-w.
Liu, Y., Iglauer, S., Cai, J., Amooie, M.A., Qin, C., 2019. Local instabilities during capillary-dominated immiscible displacement in porous media. Capillarity 2, 1–7. https://doi.org/10.26804/capi.2019.01.01.
Lo, W.-C., Yang, C.-C., Hsu, S.-Y., Chen, C.-H., Yeh, C.-L., Hilpert, M., 2017. The dynamic response of the water retention curve in unsaturated soils during drainage to acoustic excitations. Water Resour. Res. 53, 712–725. https://doi.org/10.1002/2016WR018833.
Manthey, S., Hassanizadeh, S.M., Helmig, R., 2005. Macro-scale dynamic effects in homogeneous and heterogeneous porous media. In: Das, D.B., Hassanizadeh, M.S. (Eds.), Upscaling Multiphase Flow in Porous Media. Springer, pp. 121–145. https://doi.org/10.1007/1-4020-3604-3_7.
Mason, G., Mellor, D.W., 1995. Simulation of drainage and imbibition in a random packing of equal spheres. J. Colloid Interface Sci. 176, 214–225. https://doi.org/10.1006/jcis.1995.0024.
Mueller, A.V., Hemond, H.F., 2013. Extended artificial neural networks: incorporation of a priori chemical knowledge enables use of ion selective electrodes for in-situ measurement of ions at environmentally relevant levels. Talanta 117, 112–118. https://doi.org/10.1016/j.talanta.2013.08.045.
O'Carroll, D.M., Phelan, T.J., Abriola, L.M., 2005. Exploring dynamic effects in capillary pressure in multistep outflow experiments. Water Resour. Res. 41, W11419. https://doi.org/10.1029/2005WR004010.
Oung, O., Hassanizadeh, S.M., Bezuijen, A., 2005. Two-phase flow experiments in a geocentrifuge and the significance of dynamic capillary pressure effect. J. Porous Media 8, 247–257. https://doi.org/10.1615/JPorMedia.v8.i3.10.
Qin, C., 2015. Water transport in the gas diffusion layer of a polymer electrolyte fuel cell: dynamic pore-network modeling. J. Electrochem. Soc. 162, F1036. https://doi.org/10.1149/2.0861509jes.
Rabbani, H.S., Joekar-Niasar, V., Pak, T., Shokri, N., 2017. New insights on the complex dynamics of two-phase flow in porous media under intermediate-wet conditions. Sci. Rep. 7, 4584. https://doi.org/10.1038/s41598-017-04545-4.
Raeini, A.Q., Bijeljic, B., Blunt, M.J., 2014a. Numerical modelling of sub-pore scale events in two-phase flow through porous media. Transp. Porous Media 101, 191–213. https://doi.org/10.1007/s11242-013-0239-6.
Raeini, A.Q., Blunt, M.J., Bijeljic, B., 2014b. Direct simulations of two-phase flow on micro-CT images of porous media and upscaling of pore-scale forces. Adv. Water Resour. 74, 116–126. https://doi.org/10.1016/j.advwatres.2014.08.012.
Sakaki, T., O'Carroll, D.M., Illangasekare, T.H., 2010. Direct quantification of dynamic effects in capillary pressure for drainage–wetting cycles. Vadose Zone J. 9, 424–437. https://doi.org/10.2136/vzj2009.0105.
Shan, X., Chen, H., 1993. Lattice Boltzmann model for simulating flows with multiple phases and components. Phys. Rev. E 47, 1815–1819. https://doi.org/10.1103/PhysRevE.47.1815.
Stauffer, F., 1978. Time dependence of the relations between capillary pressure, water content and conductivity during drainage of porous media. In: IAHR Symposium on Scale Effects in Porous Media.
Sweijen, T., Hassanizadeh, S.M., Chareyre, B., Zhuang, L., 2018. Dynamic pore-scale model of drainage in granular porous media: the pore-unit assembly method. Water Resour. Res. 54, 4193–4213. https://doi.org/10.1029/2017WR021769.
Swift, M.R., Orlandini, E., Osborn, W.R., Yeomans, J.M., 1996. Lattice Boltzmann simulations of liquid-gas and binary fluid systems. Phys. Rev. E 54, 5041–5052. https://doi.org/10.1103/PhysRevE.54.5041.
Tang, M., Ma, H., Lu, S., Zhan, H., Wenyue, G., 2018. The effect of a microscale fracture on dynamic capillary pressure of two-phase flow in porous media. Adv. Water Resour. 113, 272–284. 10.1016/j.advwatres.2018.01.015.
Tang, M., Zhan, H., Ma, H., Lu, S., 2019. Upscaling of dynamic capillary pressure of two-phase flow in sandstone. Water Resour. Res. 55, 426–443. https://doi.org/10.1029/2017WR022377.
Tartakovsky, A.M., Meakin, P., 2006. Pore scale modeling of immiscible and miscible fluid flows using smoothed particle hydrodynamics. Adv. Water Resour. 29, 1464–1478. https://doi.org/10.1016/j.advwatres.2005.11.014.
Thompson, K.E., 2002. Pore-scale modeling of fluid transport in disordered fibrous materials. AIChE J. 48, 1369–1389. https://doi.org/10.1002/aic.690480703.
Tian, S., Lei, G., He, S., Yang, L., 2012. Dynamic effect of capillary pressure in low permeability reservoirs. Petrol. Explor. Dev. 39, 405–411. https://doi.org/10.1016/S1876-3804(12)60057-3.
Topp, G.C., Klute, A., Peters, D.B., 1967. Comparison of water content-pressure head data obtained by equilibrium, steady-state, and unsteady-state methods. Soil Sci. Soc. Am. J. 31, 312–314. https://doi.org/10.2136/sssaj1967.03615995003100030009x.
Vidales, A.M., Riccardo, J.L., Zgrablich, G., 1998. Pore-level modelling of wetting on correlated porous media. J. Phys. D: Appl. Phys. 31, 2861–2868. https://doi.org/10.1088/0022-3727/31/20/021.
Vogel, H.-J., Tölke, J., Schulz, V.P., Krafczyk, M., Roth, K., 2005. Comparison of a lattice-Boltzmann model, a full-morphology model, and a pore network model for determining capillary pressure–saturation relationships. Vadose Zone J. 4, 380–388. https://doi.org/10.2136/vzj2004.0114.
Wildenschild, D., Hopmans, J.W., Simunek, J., 2001. Flow rate dependence of soil hydraulic characteristics. Soil Sci. Soc. Am. J. 65, 35–48. https://doi.org/10.2136/sssaj2001.65135x.
Wu, R., Kharaghani, A., Tsotsas, E., 2016a. Capillary valve effect during slow drying of porous media. Int. J. Heat Mass Tran. 94, 81–86. https://doi.org/10.1016/j.ijheatmasstransfer.2015.11.004.
Wu, R., Kharaghani, A., Tsotsas, E., 2016b. Two-phase flow with capillary valve effect in porous media. Chem. Eng. Sci. 139, 241–248. https://doi.org/10.1016/j.ces.2015.09.028.
Xu, K., Wei, W., Chen, Y., Tian, H., Xu, S., Cai, J., 2022. A pore network approach to study throat size effect on the permeability of reconstructed porous media. Water 14, 77. https://doi.org/10.3390/w14010077.
Xu, Z., Liu, H., Valocchi, A.J., 2017. Lattice Boltzmann simulation of immiscible two-

phase flow with capillary valve effect in porous media. Water Resour. Res. 53, 3770–3790. https://doi.org/10.1002/2017WR020373.
Yan, G., Li, Z., Bore, T., Galindo-Torres, S., Scheuermann, A., Li, L., 2018. Dynamic effect in capillary pressure–saturation relationship using lattice Boltzmann simulation. In: Proceedings of the 2nd International Symposium on Asia Urban GeoEngineering. https://doi.org/10.1007/978-981-10-6632-0_2.
Yuan, C., Chareyre, B., Darve, F., 2016. Pore-scale simulations of drainage in granular materials: finite size effects and the representative elementary volume. Adv. Water Resour. 95, 109–124. https://doi.org/10.1016/j.advwatres.2015.11.018.
Zhang, H., He, S., Jiao, C., Luan, G., Mo, S., Lei, G., 2015. Investigation of dynamic effect of capillary pressure in ultra-low permeability sandstones. Indian Geotech. J. 45, 79–88. https://doi.org/10.1007/s40098-014-0109-3.
Zhang, J., 2011. Lattice Boltzmann method for microfluidics: models and applications. Microfluid. Nanofluid. 10, 1–28. https://doi.org/10.1007/s10404-010-0624-1.
Zheng, J., Lei, W., Ju, Y., Wang, M., 2021. Investigation of spontaneous imbibition behavior in a 3D pore space under reservoir condition by lattice Boltzmann method. J. Geophys. Res.: Solid Earth 126, e2021JB021987. https://doi.org/10.1029/2021JB021987.
Zhou, Y., Hatzignatiou, D.G., Helland, J.O., Zhao, Y., Cai, J., 2021. Pore-scale modelling of three-phase capillary pressure curves directly in uniformly wet rock images. Geofluids 2021, 6622079. https://doi.org/10.1155/2021/6622079.
Zhuang, L., Hassanizadeh, S.M., Qin, C.-Z., de Waal, A., 2017. Experimental investigation of hysteretic dynamic capillarity effect in unsaturated flow. Water Resour. Res. 53, 9078–9088. https://doi.org/10.1002/2017WR020895.